ASEAN International Sandbox Conference 2024 AISC Proceedings, Volume 3, 2024
http://aseansandbox.org

# MHD Mixed Convection Flow and Heat Transfer due to an Inclined Stretching/Shrinking Sheet

Sumayyah Alabdulhadi[1,2*], Anuar Ishak[2], Iskandar Waini[3]

[1]Department of Mathematics, Faculty of Science, Qassim University, Qassim 52571, Saudi Arabia
[2]Department of Mathematical Sciences, Faculty of Science and Technology, Universiti Kebangsaan Malaysia (UKM), Bangi 43600, Selangor, Malaysia
[3]Fakulti Teknologi Kejuruteraan Mekanikal dan Pembuatan, Universiti Teknikal Malaysia Melaka, Hang Tuah Jaya, Durian Tunggal 76100, Melaka, Malaysia
*Corresponding author, E-mail: sabdalhady@qu.edu.sa

## Abstract

This study focuses on the numerical analysis of magnetohydrodynamic (MHD) mixed convection flow of a viscous fluid over an inclined stretching sheet. The sheet's temperature and stretching velocity are assumed to follow a power law distribution. To simplify the governing partial differential equations (PDEs), we apply similarity transformations, which transform them into ordinary differential equations (ODEs). We employ the bvp4c solver in Matlab for numerical computations. Specifically, when the buoyancy force is present and the parameter $n$ is related to $m$ as n=2m-1, we obtain similarity solutions. For a particular variant of the shrinking strength, non-unique solutions are found. It is evident from the temporal stability analysis that only one of them remains stable throughout time. The study investigates the effects of various parameters, such as velocity and temperature exponents, magnetic field strength, inclination angle, and buoyancy, on the flow and heat transfer properties, which are illustrated through graphical representations. Notable findings include that the local Nusselt numbers and skin friction coefficients decrease when the inclination angle of the stretching sheet increases, while they increase when the inclination angle of the shrinking sheet increases.

***Keywords:*** *Boundary layer flow; MHD; stretching/shrinking sheet; mixed convection; inclined plate*

## 1. Introduction

The observation of magnetohydrodynamic (MHD) flow behavior has garnered considerable attention across various engineering disciplines, such as metallurgical processes and the petroleum industry, due to its crucial role in industrial applications (Abel et al., 2012). The presence of MHD in electrically conductive fluids gives rise to a resistive force known as the Lorentz force, which significantly impacts fluid concentration and temperature. This effect delays the separation within the boundary layer and the transition from laminar to turbulent flow. Numerous researchers have incorporated magnetic field influence into their studies. For instance, Goud et al. (2020) conducted a numerical investigation of MHD boundary layer flow driven by a stretching sheet and influenced by thermal radiation, revealing that higher magnetic parameter values slow down heat transport while increasing surface shear stress. Khashi'ie et al. (2022) explored MHD boundary layer flow over a moving plate with a hybrid nanofluid, finding that an increase in the magnetic parameter led to higher heat transfer rates and an expanded critical value. Rai & Mishra (2022) recently analyzed nanofluid boundary layer flow considering slip conditions and magnetic fields, observing that the magnetic parameter enhanced temperature and concentration profiles while reducing the velocity profile. Additionally, several other studies Lu et al. (2019); Abbas et al. (2019); Amar and Kishan (2021); Senapati et al. (2022) have also considered the magnetic effect in their analyses, further highlighting its significance in this research area.

Mixed convection is a heat transfer process that combines elements of both free (natural) and forced convection. In convection, heat is transferred as a fluid moves from a hotter surface to a cooler one. Forced

convection involves the use of an external source to drive fluid motion, while free convection relies on buoyant forces resulting from density variations to create fluid movement. The significance of studying mixed convection arises from its wide-ranging applications in various industries and technologies, such as nuclear reactors, pipeline transportation, and electronic devices. Understanding this phenomenon has become increasingly important, as highlighted by the work of Wahid et al. (2022); Ishak et al. (2009) investigated the effects of mixed convection on a micropolar fluid along a vertical surface, revealing that there are multiple solutions in the assisting flow region. Similarly, Waini et al. (2020) incorporated mixed convection into their research on hybrid nanofluid flow over a vertical sheet through a porous medium, finding dual solutions in opposing flows. Meanwhile, Abbas et al. (2021) explored the simultaneous influence of thermophoretic motion and thermal radiation on mixed convection flow around a spherical surface at various circumferential regions. Numerous researchers, including Ishak (2009); Öztop et al. (2017); Daniel et al. (2017); Jamaludin et al. (2021); Jahan et al. (2021); Acharya et al. (2022) and Bejawada et al. (2022) have also contributed significantly to the study of mixed convection flow, further highlighting its importance and relevance in various scientific investigations.

Researchers have shown significant interest in investigating the phenomenon of flow over stretching surfaces due to its wide-ranging applications, such as aerodynamically extending plastic sheets, manufacturing glass fibers, and the drying and cooling processes in the paper and textile industry (Nasir et al., 2017) The initial exploration of boundary layer flow induced by a stretching surface was conducted by Cran (1970). Gupta & Gupta (1977) later extended this work to encompass scenarios involving stretching surfaces with suction or blowing. Crane's pioneering research (1970) served as a captivating foundation that spurred extensive exploration along various dimensions (Arifin et al., 2017; Hamid et al., 2019; Rasool et al., 2019; Anwar et al., 2022; and Rehman et al., 2022). In a different vein, Zaimi & Ishak (2016) made an intriguing discovery during their study of stagnation point flow over a stretching vertical surface with slip effects: they observed that increasing the slip parameter led to an enhancement in the local Nusselt number. Subsequently, Shoaib et al. (2020) conducted a numerical analysis to investigate the influence of rotation on the flow of an MHD hybrid nanofluid over a stretching sheet. Their findings suggested that increasing the rotation parameter could boost the rate of heat transfer. Additionally, Rehman et al. (2021) explored the impact of dynamic viscosity on thin film nanofluid flow induced by a stretching surface. Their conclusions indicated that an increase in the volume fraction of nanoparticles resulted in a reduction in the velocity field.

In recent times, there has been a growing focus on the study of fluid flow over inclined surfaces due to its substantial relevance in engineering and industry. This interest extends to applications in gas turbines, polymer industries, MHD power generators, chemical engineering, aeronautics, and planetary magnetospheres (Bohra, 2017). Additionally, Rafique et al. (2021) conducted an investigation into the influence of suction or injection on Casson nanofluid flow over a permeable inclined sheet. Their findings indicated that as the inclination values increased, there was an enhancement in heat transfer performance. Furthermore, Anuar et al. (2021) explored mixed convection hybrid nanofluid flow over an inclined permeable shrinking/stretching surface under the influence of suction. They observed that an increase in suction and inclination angle parameters led to an improvement in the local Nusselt number. More recently, Soomro et al. (2022) utilized $Al_2O_3 - Cu$/water hybrid nanofluid to study heat transfer and MHD flow over an inclined surface. One of their key findings was that the heat transfer rate was improved compared to conventional nanofluids. Several research papers have also delved into the boundary layer flow problem over flat plates with varying inclination angles and physical conditions (Ramesh et al., 2016; Sharma and Gupta, 2017; Ilias et al., 2020; Ahmad et al., 2021; Alabdulhadi et al., 2021; and Alabdulhadi et al., 2023)

Motivated by the previously mentioned literature, this research paper serves as an extension of the preceding investigation conducted by Ishak et al. (2008). Their study involved the numerical analysis of hydromagnetic flow and heat transfer on a vertically variable temperature surface subjected to power-law

stretching, resulting in the acquisition of a singular solution. The objective of the present study is to explore magnetohydrodynamic (MHD) mixed convection flow induced by an inclined power-law stretching/shrinking sheet while incorporating the influence of suction. This research diverges from that undertaken by Ishak et al. (2008), as we specifically examine the effects of suction on a stretching/shrinking sheet positioned at an incline, in contrast, Ishak et al. (2008) focused on a vertically stretching sheet. Additionally, this paper aims to attain a nonunique solution and subsequently conduct a stability analysis thereof.

## 2. Mathematical model

The investigation explores two-dimensional magnetohydrodynamic (MHD) mixed convection flow involving a viscous, incompressible, and electrically conducting fluid. This flow is induced by an inclined stretching/shrinking surface with an inclination angle denoted as ω. Figureure 1 provides a visual representation of the physical model used in our research. In this study, we suppose that $u_w(x)=ax^m$, in which a is a positive constant, represents the stretching surface's velocity. While the y-axis is normal to the surface, the x-direction experiences stretching. Additionally, we describe the temperature distribution on the surface using $T_w=T_\infty+bx^n$, where b is a constant, and $T_\infty$ represents the unchanged ambient temperature. Furthermore, it is assumed that the magnetic Reynolds number is sufficiently low, such that the induced magnetic field can be considered negligible in our analysis.

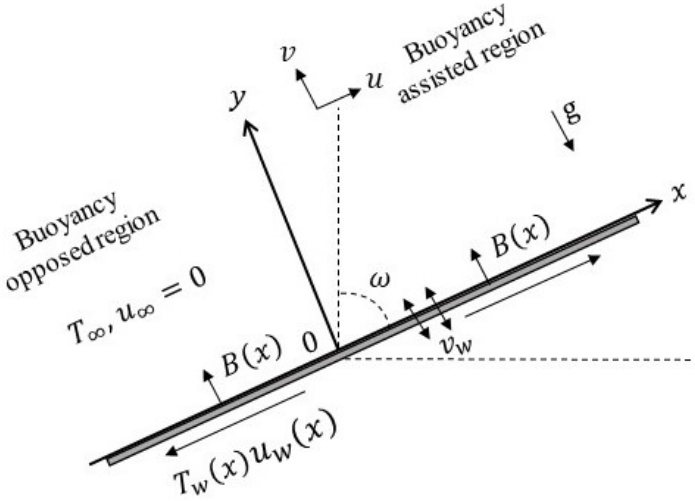


**Figure 1.** Diagram of the flow problem.

The governing equations under these presumptions, coupled with Boussinesq as well as boundary layer approximations, are (see Ishak et al., 2008 and Alabdulhadi et al., 2021)

$$\frac{\partial u}{\partial x}+\frac{\partial v}{\partial y}=0, \tag{1}$$

$$u\frac{\partial u}{\partial x}+v\frac{\partial u}{\partial y}=\nu\frac{\partial^2 u}{\partial y^2}-\frac{\sigma B^2(x)}{\rho}u+g\beta(T-T_\infty)\cos\omega, \tag{2}$$

$$u\frac{\partial T}{\partial x}+v\frac{\partial T}{\partial y}=\alpha\frac{\partial^2 T}{\partial y^2}, \tag{3}$$

subject to the boundary conditions

$$u=u_w(x)\xi,\quad v=v_w,\quad T=T_w(x)\quad at\quad y=0,$$
$$u\to 0,\quad T\to T_\infty\quad as\quad y\to\infty. \tag{4}$$

In which the components of the velocity along the y and $x$ directions are resembled by $v$ and $u$, respectively. In addition,

refers to the fluid temperature, B(x) expresses the variable magnetic field strength, g signifies the gravitational acceleration, and α denotes the fluid's thermal diffusivity. The stretching/shrinking sheet is characterised by the parameter ξ, where ξ>0 and ξ<0 denote the stretching and shrinking sheets, respectively. By contrast, the static surface is indicated by ξ=0. Additionally, ν symbolizes the kinematic viscosity, then β implies the thermal expansion's coefficient, ρ represents the fluid density, as well as $\omega$ denotes the inclination angle.

Eqs. (1)-(4)'s similarity solutions can be found by assuming that the variable magnetic field B(x) is of form $B(x)=B_0x^{(m-1)/2}$. Among several others, Chiam (1995), Anjali Devi and Thiyagarajan (2006) and Ishak et al. (2008) have also taken into account this version of B(x). The following transformation can convert Eqs. (1)-(4) into the comparable ordinary differential equations (ODEs) Ishak et al. (2008)

$$\psi=\sqrt{\nu x u_w(x)}f(\eta),\ \eta=\sqrt{\frac{u_w(x)}{\nu x}}y,\ \theta(\eta)=\frac{T-T_\infty}{T_w-T_\infty}. \tag{5}$$

Here, η represents the similarity variable. In contrast, ψ resembles the stream function with $u=\partial\psi/\partial y$ and $v=-\partial\psi/\partial x$. Here, θ and f resemble the dimensionless temperature as well as velocity, accordingly. Substituting the similarity variables (5) into Eqs. (1)-(3), the ODEs are attained, while Eq. (1) is entirely met.

$$f'''+\frac{m+1}{2}ff''-mf'^2-Mf'+\lambda\theta\cos\omega=0, \tag{6}$$

$$\frac{1}{Pr}\theta''+\frac{m+1}{2}f\theta'-nf'\theta=0, \tag{7}$$

in which $Pr=\frac{\nu}{\alpha}$ measures the Prandtl number as well $M=\sigma B_0^2/(\rho a)$ demonstrates the magnetic parameter. Furthermore, $\lambda=Gr_x/Re_x^2$ represents the mixed convection parameter, in which $Re_x=u_wx/\nu$ denotes the local Reynolds number, as well as $Gr_x=g\beta(T_w-T_\infty)x^3/\nu^2$ denotes the number of the local Grashof. If $n=2m-1$, it can be demonstrated that $\lambda$ is independent with respect to $x$. Therefore, the similarity solutions are attained under this limitation when $\lambda\neq 0$. Note that opposing and assisting flows are resembled by $\lambda<0$ and $\lambda>0$, respectively. Additionally, the forced convection flow is indicated by $\lambda=0$. Eq. (7) is transformed as below under the limitation $n=2m-1$

$$\frac{1}{Pr}\theta''+\frac{m+1}{2}f\theta'-(2m-1)f'\theta=0, \tag{8}$$

the transformed conditions are

$$f(0)=s,\quad f'(0)=\xi,\quad \theta(0)=1,$$
$$f'(\eta)\to 0,\quad \theta(\eta)\to 0,\ as\quad \eta\to\infty. \tag{9}$$

The physical quantities with regard to the practical significance are the skin friction coefficient $C_f$, including the local Nusselt number $Nu_x$, which are defined given as follows

$$C_f=\frac{\tau_w}{\rho U^2/2},\ Nu_x=\frac{xq_w}{k(T_w-T_\infty)}, \tag{10}$$

given that $\tau_w$ connotes the skin friction or shear stress, whilst $q_w$ represents heat transfer from the sheet, where

$$\tau_w=\mu\left(\frac{\partial u}{\partial y}\right)_{y=0},\ q_w=-k\left(\frac{\partial T}{\partial y}\right)_{y=0}, \tag{11}$$

having $k$ and $\mu$ express the thermal conductivity as well as dynamic viscosity, respectively. Inserting Eq. (5) into Eq. (10) and using Eq. (11), one obtains

$$\frac{1}{2}C_f Re_x^{1/2}=f''(0),\ Nu_x/Re_x^{1/2}=-\theta'(0). \tag{12}$$

## 3. Materials and Methods

### *Stability Analysis*

The numerical observations suggest the existence of two solutions for certain values of the parameters. In order to ascertain the stability of these solutions over time, it becomes imperative to investigate which one remains stable during the temporal evolution. To perform a stability analysis for both solutions, following the approach outlined by Weidman et al. (2006), it is necessary to consider the problem in an unsteady form by introducing a dimensionless time parameter $\tau$. The unsteady formulation of the governing Eqs. (2) and (3) can be expressed as follows:

$$\frac{\partial u}{\partial t}+u\frac{\partial u}{\partial x}+v\frac{\partial u}{\partial y}=\nu\frac{\partial^2 u}{\partial y^2}-\frac{\sigma B^2(x)}{\rho}u+g\beta(T-T_\infty)\cos\omega, \tag{13}$$

$$\frac{\partial T}{\partial t}+u\frac{\partial T}{\partial x}+v\frac{\partial T}{\partial y}=\alpha\frac{\partial^2 T}{\partial y^2}, \tag{14}$$

where $t$ denotes the time, the new similarity transformation is articulated as follows:

$$\psi=\sqrt{\nu x u_w(x)}f(\eta,\tau),\ \eta=\sqrt{\frac{u_w(x)}{\nu x}}y,\ \theta(\eta,\tau)=\frac{T-T_\infty}{T_w-T_\infty},\quad \tau=at. \tag{15}$$

By integrating Eq. (15) into Eqs. (13) and (14), a subsequent set of equations is obtained

$$\frac{\partial^3 f}{\partial\eta^3}+\frac{m+1}{2}f\frac{\partial^2 f}{\partial\eta^2}-m\left(\frac{\partial f}{\partial\eta}\right)^2-M\frac{\partial f}{\partial\eta}+\lambda\theta\cos\omega-\frac{\partial^2 f}{\partial\eta\partial\tau}=0, \tag{16}$$

$$\frac{1}{Pr}\frac{\partial^2\theta}{\partial\eta^2}+\frac{m+1}{2}f\frac{\partial\theta}{\partial\eta}-n\frac{\partial f}{\partial\eta}\theta-\frac{\partial\theta}{\partial\tau}=0, \tag{17}$$

the succeeding initial and boundary conditions are delineated as follows:

$$f(0,\tau)=s,\quad \frac{\partial f}{\partial\eta}(0,\tau)=\xi,\quad \theta(0,\tau)=1,$$
$$\frac{\partial f}{\partial\eta}(\eta,\tau)\to 0,\quad \theta(\eta,\tau)\to 0,\ \text{as}\quad \eta\to\infty. \tag{18}$$

In order to examine the flow's long-term stability, perturbations are added using $f(\eta)=f_0(\eta)$ and $\theta(\eta)=\theta_0(\eta)$. According to the guidelines in Weidman et al. (2006), these perturbations follow Eqs. (16) and (17):

$$f(\eta,\tau)=f_0(\eta)+e^{-\gamma\tau}F(\eta,\tau),\ \theta(\eta,\tau)=\theta_0(\eta)+e^{-\gamma\tau}G(\eta,\tau) \quad (19)$$

an unknown eigenvalue is represented by the value $\gamma$. Through the integration of Eq. (19) into Eqs (16)–(18), the linearized problems are obtained:

$$F_0'''+\frac{m+1}{2}(f_0F_0''+F_0f_0'')+\lambda G_0\cos\omega-(2mf_0'-\gamma+M)F_0'=0, \quad (20)$$

$$\frac{1}{Pr}G_0''+\frac{m+1}{2}\left(f_0G_0'+F_0\theta_0'\right)-n\left(f_0'G_0-F_0'\theta_0\right)+\gamma G_0=0, \quad (21)$$

subject to

$$F_0'(0)=0,\quad F_0(0)=0,\quad G_0(0)=0,$$
$$F_0'(\eta)\to 0,\quad G_0(\eta)\to 0,\ \text{as}\quad \eta\to\infty. \quad (22)$$

For the steady flow solutions $f_0(\eta)$ and $\theta_0(\eta)$, the smallest eigenvalue $\gamma$ determines their stability. To obtain potential eigenvalues, one must loosen the boundary condition on $F(\eta)$ or $G(\eta)$, in accordance with Harris et al. (2009). Hence, the constraint $F_0'(\eta)\to 0$ is relaxed as $\eta\to\infty$ and the system (20)–(22) are resolved with the new boundary condition $F_0''=1$.

## 4. Results

The nonlinear ordinary differential equations (ODEs) described by Eqs. (6) and (8), along with the boundary condition in Eq. (9), were investigated using numerical analysis for the inclined stretching sheet. The bvp4c solver in Matlab software, as referenced in Shampine et al. (2003), was utilized for this purpose. Specifically, we explored the behavior of the system for non-zero buoyancy force ($\lambda \neq 0$) under the constraint that the temperature exponent parameter n is related to the velocity exponent parameter $m$ as n=2m-1. This relationship leads to similarity solutions for the considered problem.

In the numerical computations, we consistently set the Prandtl number to unity for simplicity, except for comparisons with previously studied cases. The obtained numerical solutions for the local Nusselt number, denoted as $-\theta'(0)$, were validated by comparing them with the findings of Grubka & Bobba (1985) and Ishak et al. (2008) across various parameter values, as summarized in Table 1. This validation instills a high level of confidence in the accuracy and agreement of our current numerical results with existing research. Furthermore, Table 2 illustrates the influence of the magnetic parameter M on both $f''(0)$ and $-\theta'(0)$ when Pr=1, $\lambda$=1, $\omega=\pi/4$, m=1 and n=1. It is evident from the table that as the magnetic parameter M increases, both the coefficient of skin friction $f''(0)$ and the local Nusselt number $-\theta'(0)$ decrease.

**Table 1.** Values of $-\theta'(0)$ for $\lambda$=0, $\omega$=0, M=0, m=1 and various values of Pr and n.

| n | Grubka & Bobba [47] | | Ishak et al. [41] | | Present result | |
|---|---|---|---|---|---|---|
| | **Pr=1** | **Pr=3** | **Pr=1** | **Pr=3** | **Pr=1** | **Pr=3** |
| -2 | -1.0000 | -3.0000 | -1.0000 | -3.0000 | -1.0000 | -3.0000 |
| -1 | 0.0 | 0.0 | 0.0 | 0.0 | 0.0 | 0.0 |
| 0 | 0.5820 | 1.1652 | 0.5820 | 1.1652 | 0.5820 | 1.1652 |
| 1 | 1.0000 | 1.9237 | 1.0000 | 1.9237 | 1.0000 | 1.9237 |
| 2 | 1.3333 | 2.5097 | 1.3333 | 2.5097 | 1.3333 | 2.5097 |

**Table 2.** Numerical values of $f''(0)$ and $-\theta'(0)$ for a variety of values for M when Pr=1, λ=1, $\omega = \pi/4$, m=1 and n=1.

| M | $f''(0)$ | $-\theta'(0)$ |
|---|---|---|
| 0 | -0.796273 | 1.149875 |
| 0.1 | -0.841299 | 1.140629 |
| 0.2 | -0.885012 | 1.131634 |
| 0.5 | -1.009140 | 1.106036 |
| 1 | -1.196730 | 1.067385 |
| 2 | -1.520101 | 1.001717 |
| 5 | -2.263094 | 0.861678 |

Figure 2 depict the impact of the parameter $\omega$ on the skin friction coefficient $Re_x^{1/2}C_f$ and the local Nusselt number $Re_x^{-1/2}Nu_x$ in relation to $\xi$, with given parameters Pr=1, M=1, λ=-1.5, m=1 and s=2.5. It is worth noting that within the region of shrinking ($\xi>\xi_c$), specific parameter levels give rise to dual solutions, while a singular solution emerges at the critical value $\xi_c$. However, for values of $\xi$ smaller than $\xi_c$, no solutions are found, where $\xi_c$ signifies the convergence of solutions. These Figureures demonstrate that higher values of $\omega$ lead to increased values of both $Re_x^{1/2}C_f$ and $Re_x^{-1/2}Nu_x$. This physical observation indicates a more significant buoyancy effect in the opposing flow region (λ<0) as ω increases. Consequently, with the intensified buoyancy force, both $Re_x^{1/2}C_f$ and $Re_x^{-1/2}Nu_x$ exhibit an upward trend. Additionally, an inverse relationship is observed between the critical value of the stretching/shrinking parameter ξ and the increasing value of ω. The critical values of ξ for ω=0°, 45° and 60° are -2.85415, -2.97862, and -3.07546, respectively.

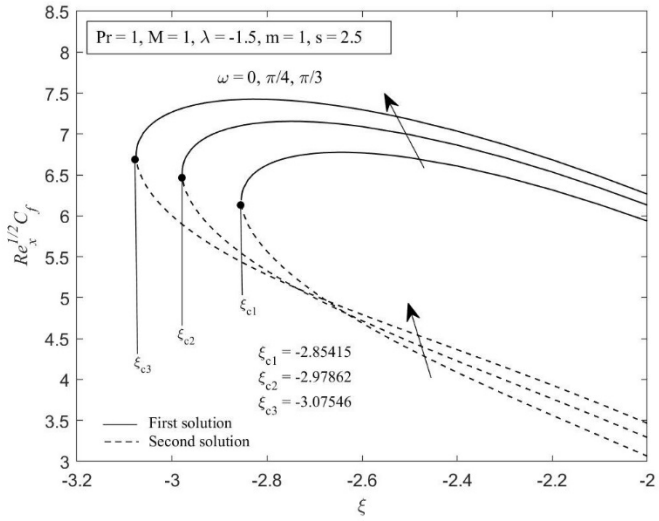


(a)

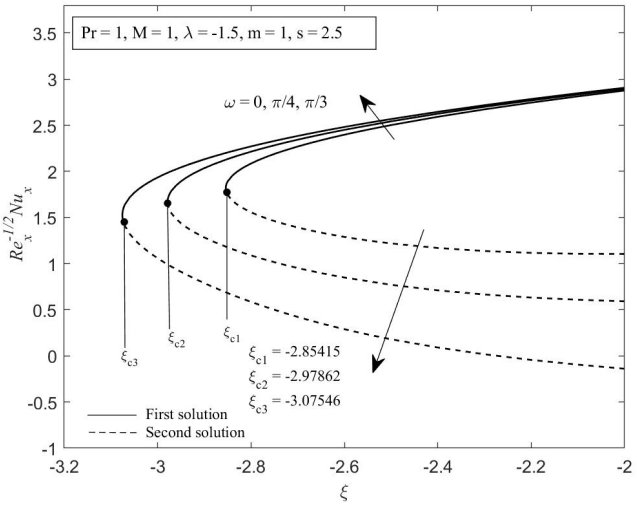


(b)

**Figure 2.** $Re_x^{1/2}C_f$ and $Re_x^{-1/2}Nu_x$ with ξ for diverse values of ω.

Figure 3 illustrate the velocity and temperature profiles for various values of $\omega$, while considering the given parameters Pr=1, M=1, $\lambda = -1.5$, $\xi = -2.5$, $m = 1$ and $s = 2.5$. These Figureures exhibit the presence of two distinct solutions for both velocity and temperature profiles, which closely adhere to the conditions (8), thereby verifying the credibility of the numerical findings. In Figure. 3a, it is apparent that the first solution witnesses an augmentation in velocity as $\omega$ increases, whereas the second solution follows a different pattern. Similarly, Figure. 3b indicates that an escalation in $\omega$ leads to a decrease in temperature for the first solution, while the second solution displays an inclination towards increasing temperature. Furthermore, when the plate undergoes a transition from a vertical to a horizontal position (accompanied by an increase in ω) in the opposing flow region, the buoyancy force intensifies. Consequently, the thickness of the velocity boundary layer expands, while the thickness of the thermal boundary layer diminishes. As a result, there is an increment in the values of $f'(\eta)$ and a corresponding reduction in the values of $\theta(\eta)$. It is noteworthy that the problem simplifies to a vertical plate when ω is $0^{\circ}$, a horizontal plate at $90^{\circ}$, and an inclined plate at $30^{\circ}$, $45^{\circ}$, and $60^{\circ}$.

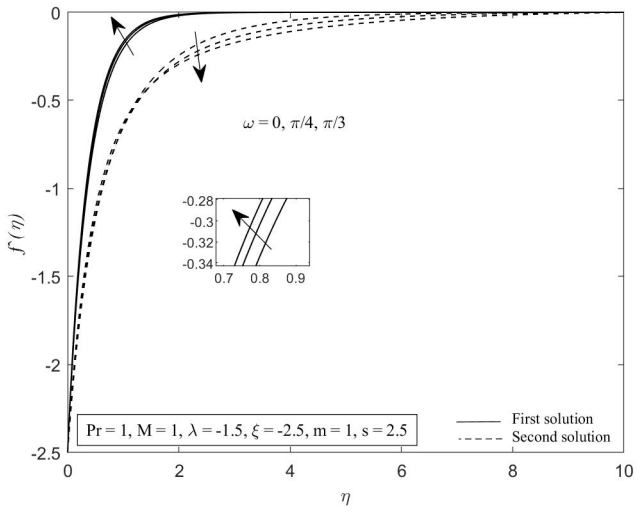


(a)

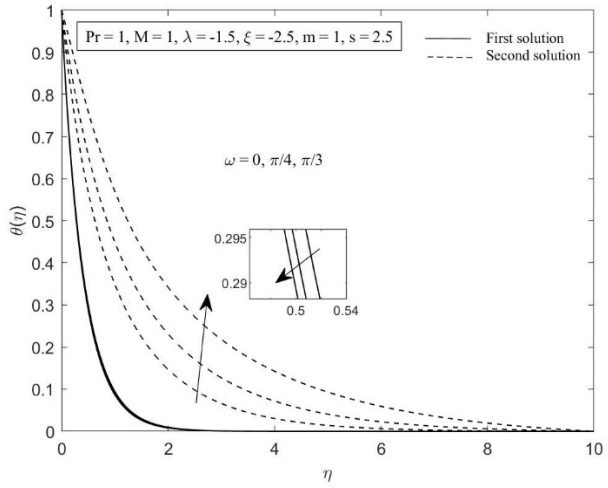


(b)

**Figure 3.** $f'(\eta)$ and $\theta(\eta)$ for diverse values of ω.

Figure 4 shows the impact of the inclination angle parameter $\omega$ on the skin friction coefficient $f''(0)$ and the local Nusselt number $-\theta'(0)$ in relation to the parameter λ. This analysis assumes Pr=1, M=1, ξ=1, m=1 and n=1. In these Figures, it is evident that when the buoyancy force is small, the $f''(0)$ value is negative for a specific ω value. However, it can become positive when the buoyancy force is strong enough. For λ<0, there is no solution, while all solutions converge at λ=0. Furthermore, as ω increases, Figureure 4 show a decrease in both $f''(0)$ and $-\theta'(0)$. This decrease is expected because the buoyancy effect intensifies with higher $\omega$, due to thermal changes in the assisting flow region (λ>0). Thus, as the assisting buoyancy force increases, the values of $f''(0)$ and $-\theta'(0)$ decrease.

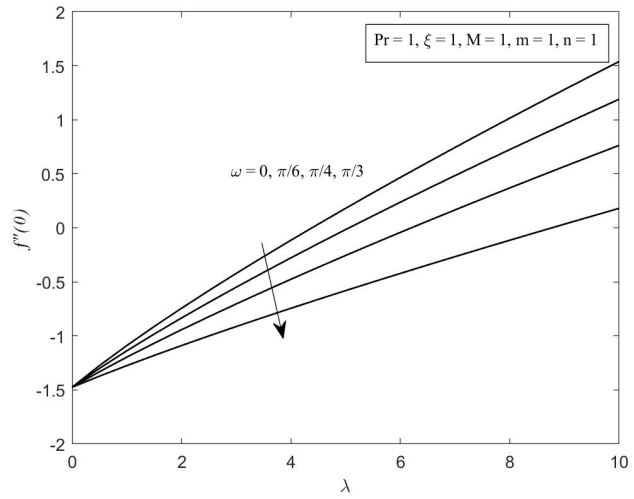


(a)

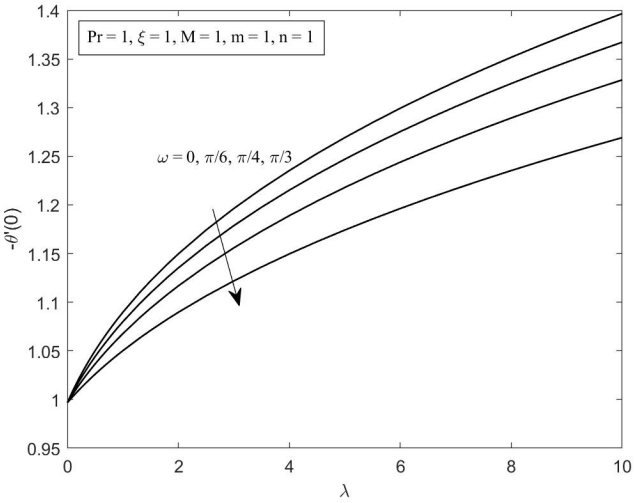


(b)

**Figure 4.** $f''(0)$ and $-\theta'(0)$ with λ for diverse values of ω.

Figure. 5 illustrate how changes in the inclination angle parameter $\omega$ affect the velocity and temperature profiles when Pr=1, M=1, ξ=1, λ=1, m=1 and n=1. These Figures reveal that increasing ω has contrasting effects on velocity and temperature profiles. When ω rises, the velocity profile decreases, while the temperature profile increases. This behavior can be explained by the maximal gravitational force's impact when the surface is oriented vertically. Furthermore, as the plate is tilted from vertical to horizontal (i.e., as ω increases), the assisting buoyancy force grows. This results in a thinner velocity boundary layer, a thicker thermal boundary layer, a decrease in velocity profile, and an increase in temperature profile.

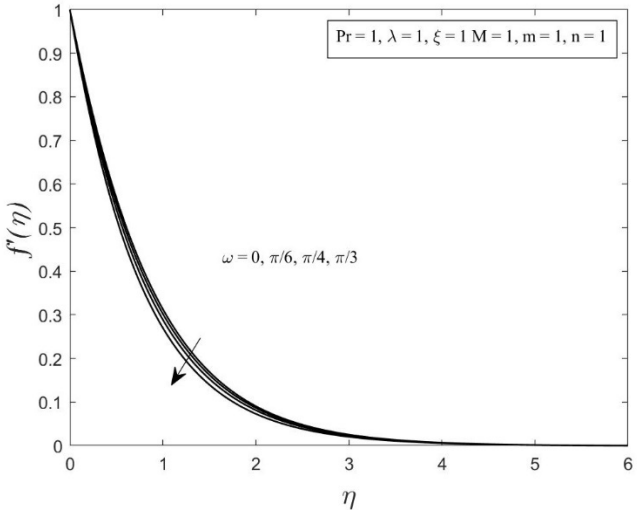


(a)

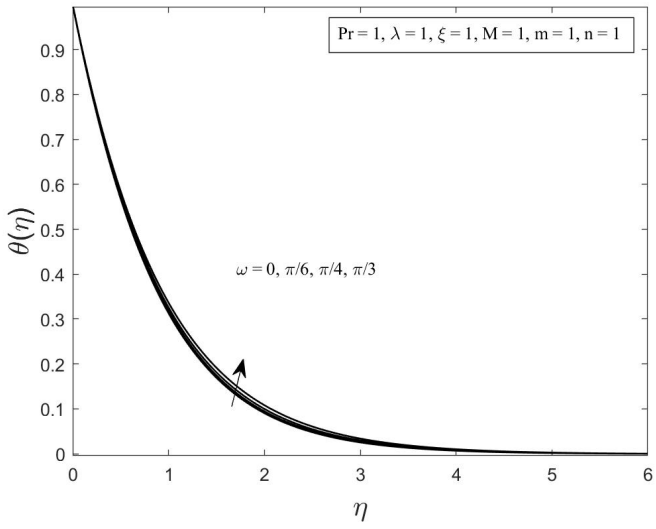


(b)

**Figure 5.** $f'(\eta)$ and $\theta(\eta)$ for diverse values of ω.

Moving on to the influence of m (and n) on the skin friction coefficient $f''(0)$ and the local Nusselt number $-\theta'(0)$ concerning the parameter λ, we consider Pr=1, M=1, ξ=1, and $\omega=\pi/4$. In Figure. 6, similar to the variation with ω, there is no solution for the opposing flow ($\lambda<0$) in this scenario. When λ=0 (indicating the absence of buoyancy force), the value of $f''(0)$ is consistently negative, regardless of the specific conditions, Pr=1, M=1, and $\omega=\pi/4$. In a physical sense, these negative values of $f''(0)$ signify that the sheet imposes a drag force on the fluid. Conversely, positive values of $f''(0)$ indicate the opposite. The occurrence of negative $f''(0)$ values when λ=0 is expected since, in this case, the stretching sheet is the sole factor contributing to the creation of the boundary layer. However, it's worth noting that regardless of the presence or absence of the buoyancy force, the local Nusselt number $-\theta'(0)$ remains positive, implying that heat is

transferred from the hot sheet to the cooler fluid. Furthermore, Figure. 6b illustrates that as both the buoyancy parameter λ and the velocity exponent parameter m increase, the heat transfer rate at the surface also increases.

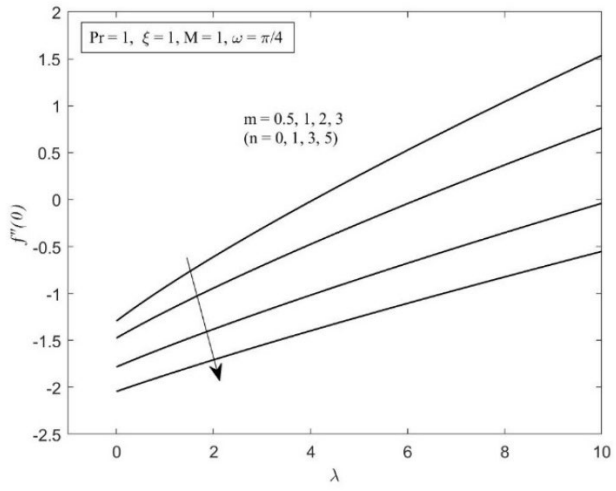


(a)

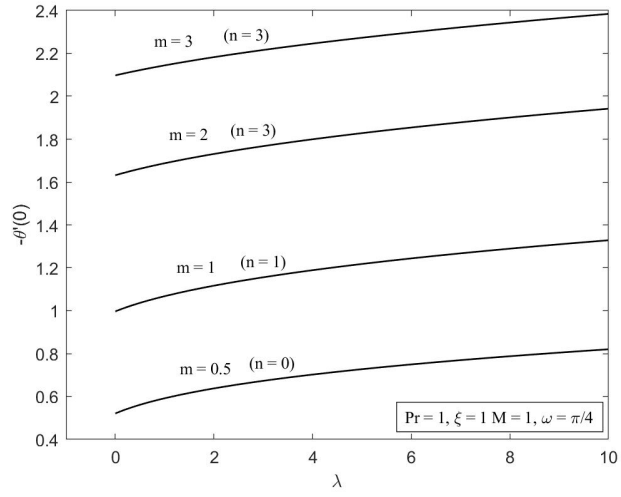


(b)

**Figure 6.** $f''(0)$ and $-\theta'(0)$ with λ for diverse values of m (and n).

In Figure 7, we observe how the velocity exponent parameter m, which includes the temperature exponent parameter n, affects velocity and temperature profiles when Pr=1, M=1, ξ=1, λ=1 and ω=π/4. Increasing the parameter m leads to a decrease in both velocity and temperature profiles within the boundary layers. Consequently, the velocity and temperature boundary layer thicknesses decrease as m increases. Figure. 7 also demonstrates that the far-field boundary conditions (9) support the validity of the numerical results and are asymptotically met.

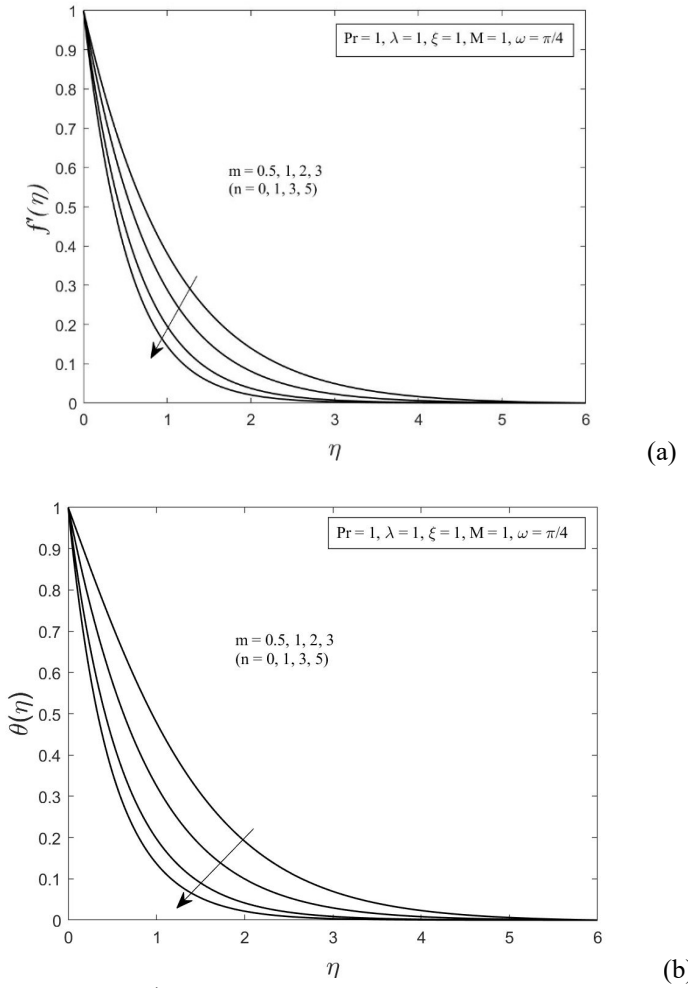


**Figure 7.** $f'(\eta)$ and $\theta(\eta)$ for diverse values of m (and n).

Finally, by utilizing the bvp4c function within MATLAB, an analysis of stability is performed to solve Eqs. (20)-(22). The depiction of the smallest eigenvalues $\gamma$ when Pr=1, M=1, $\lambda$=-1.5, $\omega=\pi/4$, m=1 and s=2.5 for different values of $\xi$ is shown in Figure. 8. The importance of these eigenvalues resides in their ability to evaluate the stability of dual solutions. A positive value for the smallest eigenvalue $\gamma$ signifies stability, indicating minimal disturbances that have an insignificant impact on the flow characteristics or physical appearance. Conversely, a negative value for the smallest eigenvalues denotes instability, suggesting that disturbances affecting the flow system are increasing. Furthermore, it can be deduced from Figure. 8 that the first solution remains stable over time, while the other solution does not.

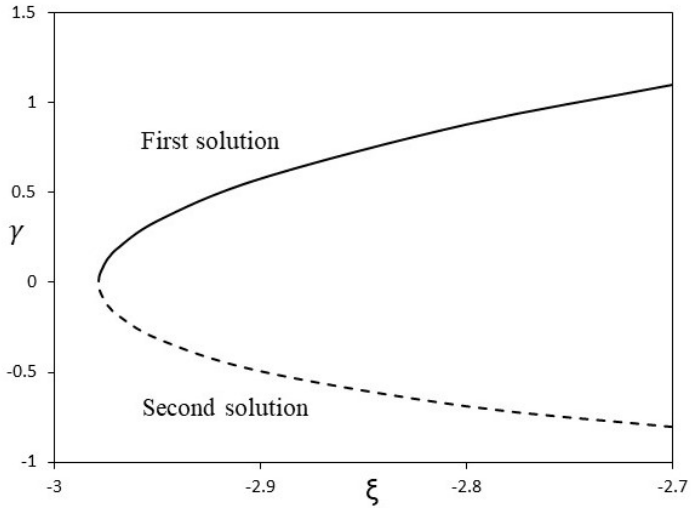


**Figure 8.** Eigenvalue $\gamma$

with $\xi$ when Pr=1, M=1, $\lambda$=-1.5, $\omega=\pi/4$, m=1 and s=2.5

## 5. Conclusion

In this study, we have conducted a numerical investigation of the magnetohydrodynamic mixed convection flow of a viscous fluid generated by an inclined stretching/shrinking sheet. Our analysis considered various crucial parameters, such as M, m, n, $\omega$ and $\lambda$. The numerical results were obtained using the bvp4c solver in Matlab, and the key findings can be summarized as follows:

- Dual solutions are identified within a specific range of shrinking strength ($\xi_c<\xi<1$).
- Temporal stability analysis reveals that only the first solution exhibits stability.
- The skin friction coefficient and heat transfer across an inclined shrinking surface increase with higher values of $\omega$.
- An increase in the inclination angle parameter results in a decrease in the velocity profile and an increase in the temperature profile in the assisting flow region, while the opposing flow region exhibits the opposite trend.
- Large values of the velocity exponent parameter lead to reductions in temperature and velocity fields.
- When there is a buoyancy force and n=2m-1, similarity solutions are obtained.
- The magnetic parameter substantially reduces both skin friction and the local Nusselt number.
- Skin friction and the local Nusselt number decrease with increasing angle of inclination, while a notable increasing effect is observed with higher values of the buoyancy parameter in the assisting flow.
- An increase in the velocity exponent parameter is associated with a decrease in $f''(0)$ and an increase in $-\theta'(0)$.

**Author Contributions:** Conceptualization, A.I.; funding acquisition, A.I.; methodology, S.A. and I.W.; Supervision, A.I.; validation, I.W.; writing—original draft, S.A.; writing—review and editing, A.I. All authors have read and agreed to the published version of the manuscript.
**Institutional Review Board Statement:** Not applicable.
**Informed Consent Statement:** Not applicable.
**Informed Consent Statement:** Not applicable. Conflicts of Interest: The authors declare no conflict of interest.

**References**

Abbas, A., Ashraf, M., & Chamkha, A. J. (2021). Combined effects of thermal radiation and thermophoretic motion on mixed convection boundary layer flow. *Alexandria Engineering Journal*, *60*(3), 3243-3252.

Abbas, Z., Abdal, S., Hussain, N., Hussain, F., Adnan, M., Ali, B., Zulqarnain, R.M., Ali, L., & Younas, S. (2019). Mhd boundary layer flow and heat transfer of nanofluid over a vertical stretching sheet in the presence of a heat source. *Scientific Inquiry and Review*, *3*(4), 60-73.

Abel, M. S., Tawade, J. V., & Shinde, J. N. (2012). The effects of MHD flow and heat transfer for the UCM fluid over a stretching surface in presence of thermal radiation. *Advances in Mathematical Physics*, *2012*(1), 702681.

Acharya, N., Mabood, F., & Badruddin, I. A. (2022). Thermal performance of unsteady mixed convective Ag/MgO nanohybrid flow near the stagnation point domain of a spinning sphere. *International Communications in Heat and Mass Transfer*, *134*, 106019.

Ahmad, F., Nazeer, M., Ali, W., Saleem, A., Sarwar, H., Suleman, S., & Abdelmalek, Z. (2021). Analytical study on couple stress fluid in an inclined channel. *Scientia Iranica*, *28*(4), 2164-2175.

Alabdulhadi, S., Abu Bakar, S., Ishak, A., Waini, I., & Ahmed, S. E. (2023). Effect of buoyancy force on an unsteady thin film flow of Al2O3/water nanofluid over an inclined stretching sheet. *Mathematics*, *11*(3), 739.

Alabdulhadi, S., Waini, I., Ahmed, S. E., & Ishak, A. (2021). Hybrid nanofluid flow and heat transfer past an inclined surface. *Mathematics*, *9*(24), 3176.

Amar, N., & Kishan, N. (2021). The influence of radiation on MHD boundary layer flow past a nano fluid wedge embedded in porous media. *Partial Differential Equations in Applied Mathematics*, *4*, 100082.

Anjali Devi, S. P., & Thiyagarajan, M. (2006). Steady nonlinear hydromagnetic flow and heat transfer over a stretching surface of variable temperature. *Heat and Mass Transfer*, *42*, 671-677.

Anuar, N. S., Bachok, N., & Pop, I. (2021). Influence of buoyancy force on Ag-MgO/water hybrid nanofluid flow in an inclined permeable stretching/shrinking sheet. *International Communications in Heat and Mass Transfer*, *123*, 105236.

Anwar, M. I., Firdous, H., Zubaidi, A. A., Abbas, N., & Nadeem, S. (2022). Computational analysis of induced magnetohydrodynamic non-Newtonian nanofluid flow over nonlinear stretching sheet. *Progress in Reaction Kinetics and Mechanism*, *47*, 14686783211072712.

Arifin, N. S., Zokri, S. M., Kasim, A. R. M., Salleh, M. Z., Mohammad, N. F., & Yusoff, W. N. S. W. (2017, September). Aligned magnetic field of two-phase mixed convection flow in dusty Casson fluid over a stretching sheet with Newtonian heating. In *Journal of Physics: Conference Series* (Vol. 890, No. 1, p. 012001). IOP Publishing.

Bejawada, S. G., Reddy, Y. D., Jamshed, W., Eid, M. R., Safdar, R., Nisar, K. S., ... & Parvin, S. (2022). 2D mixed convection non-Darcy model with radiation effect in a nanofluid over an inclined wavy surface. *Alexandria Engineering Journal*, *61*(12), 9965-9976.

Bohra, S. (2017). Heat and mass transfer over a three-dimensional inclined non-linear stretching sheet with

convective boundary conditions. *Indian Journal of Pure & Applied Physics (IJPAP)*, *55*(12), 847-856.

Chiam, T. C. (1995). Hydromagnetic flow over a surface stretching with a power-law velocity. *International journal of engineering science*, *33*(3), 429-435.

Crane, L. J. (1970). Flow past a stretching plate. *Zeitschrift für angewandte Mathematik und Physik ZAMP*, *21*, 645-647.

Daniel, Y. S., Aziz, Z. A., Ismail, Z., & Salah, F. (2017). Double stratification effects on unsteady electrical MHD mixed convection flow of nanofluid with viscous dissipation and Joule heating. *Journal of applied research and technology*, *15*(5), 464-476.

Goud, B. S., Srilatha, P., Bindu, P., & Krishna, Y. H. (2020). Radiation effect on MHD boundary layer flow due to an exponentially stretching sheet. *Advances in Mathematics: Scientific Journal*, *9*(12), 10755-10761.

Grubka, L. J., & Bobba, K. M. (1985). Heat transfer characteristics of a continuous stretching surface with variable temperature. *Journal of Heat Transfer*, *107*(1), 248-250.

Gupta, P. S., & Gupta, A. S. (1977). Heat and mass transfer on a stretching sheet with suction or blowing. *The Canadian journal of chemical engineering*, *55*(6), 744-746.

Hamid, M., Usman, M., Khan, Z. H., Ahmad, R., & Wang, W. (2019). Dual solutions and stability analysis of flow and heat transfer of Casson fluid over a stretching sheet. *Physics Letters A*, *383*(20), 2400-2408.

Harris, S. D., Ingham, D. B., & Pop, I. (2009). Mixed convection boundary-layer flow near the stagnation point on a vertical surface in a porous medium: Brinkman model with slip. *Transport in Porous Media*, *77*, 267-285.

Ilias, M. R., Ismail, N. S. A., AbRaji, N. H., Rawi, N. A., & Shafie, S. (2020). Unsteady aligned MHD boundary layer flow and heat transfer of a magnetic nanofluids past an inclined plate. *International Journal of Mechanical Engineering and Robotics Research*, *9*(2), 197-206.

Ishak, A. (2009). Mixed convection boundary layer flow over a vertical cylinder with prescribed surface heat flux. *Journal of Physics A: Mathematical and Theoretical*, *42*(19), 195501.

Ishak, A., Nazar, R., & Pop, I. (2008). Hydromagnetic flow and heat transfer adjacent to a stretching vertical sheet. *Heat and Mass Transfer*, *44*(8), 921-927.

Ishak, A., Nazar, R., & Pop, I. (2009). Dual solutions in mixed convection boundary layer flow of micropolar fluids. *Communications in Nonlinear Science and Numerical Simulation*, *14*(4), 1324-1333.

Jahan, S., Ferdows, M., Shamshuddin, M., & Zaimi, K. (2021). Radiative mixed convection flow over a moving needle saturated with non-isothermal hybrid nanofluid. *Journal of Advanced Research in Fluid Mechanics and Thermal Sciences*, *88*(1), 81-93.

Jamaludin, A., Nazar, R., Naganthran, K., & Pop, I. (2021). Mixed convection hybrid nanofluid flow over an exponentially accelerating surface in a porous media. *Neural Computing and Applications*, *33*(22), 15719-15729.

Khashi'ie, N. S., Arifin, N. M., & Pop, I. (2022). Magnetohydrodynamics (MHD) boundary layer flow of hybrid nanofluid over a moving plate with Joule heating. *Alexandria Engineering Journal*, *61*(3), 1938-1945.

Lu, D., Mohammad, M., Ramzan, M., Bilal, M., Howari, F., & Suleman, M. (2019). MHD boundary layer flow of Carreau fluid over a convectively heated bidirectional sheet with non-Fourier heat flux and variable thermal conductivity. *Symmetry*, *11*(5), 618.

Nasir, N. A. A. M., Ishak, A., & Pop, I. (2017). Stagnation-point flow and heat transfer past a permeable quadratically stretching/shrinking sheet. *Chinese Journal of Physics*, *55*(5), 2081-2091.

Öztop, H. F., Sakhrieh, A., Abu-Nada, E., & Al-Salem, K. (2017). Mixed convection of MHD flow in

nanofluid filled and partially heated wavy walled lid-driven enclosure. *International Communications in Heat and Mass Transfer*, *86*, 42-51.

Rafique, K., Imran, M. A., Anwar, M. I., Misiran, M., & Ahmadian, A. (2021). Energy and mass transport of Casson nanofluid flow over a slanted permeable inclined surface. *Journal of Thermal Analysis and Calorimetry*, *144*, 2031-2042.

Rai, P., & Mishra, U. (2022). Numerical Simulation of Boundary Layer Flow Over a Moving Plate in The Presence of Magnetic Field and Slip Conditions. *Journal of Advanced Research in Fluid Mechanics and Thermal Sciences*, *95*(2), 120-136.

Ramesh, G. K., Chamkha, A. J., & Gireesha, B. J. (2016). Boundary layer flow past an inclined stationary/moving flat plate with convective boundary condition. *Afrika Matematika*, *27*, 87-95.

Rasool, G., Shafiq, A., Khalique, C. M., & Zhang, T. (2019). Magnetohydrodynamic Darcy–Forchheimer nanofluid flow over a nonlinear stretching sheet. *Physica Scripta*, *94*(10), 105221.

Rehman, A., Salleh, Z., & Gul, T. (2021). Heat transfer of thin film flow over an unsteady stretching sheet with dynamic viscosity. *Journal of Advanced Research in Fluid Mechanics and Thermal Sciences*, *81*(2), 67-81.

Rehman, S., Gul, T., Khan, W., Khan, A., & Zeeshan. (2022). Effects of chemical reaction, viscosity, thermal conductivity, heat source, radiation/absorption, on MHD mixed convection nano-fluids flow over an unsteady stretching sheet by HAM and numerical method. *Advances in Mechanical Engineering*, *14*(1), 16878140221074301.

Senapati, M., Parida, S. K., Swain, K., & Ibrahim, S. M. (2022). Analysis of variable magnetic field on chemically dissipative MHD boundary layer flow of Casson fluid over a nonlinearly stretching sheet with slip conditions. *International Journal of Ambient Energy*, *43*(1), 3712-3726.

Shampine, L. F., Gladwell, I., & Thompson, S. (2003). *Solving ODEs with matlab*. New York: Cambridge university press.

Sharma, K., & Gupta, S. (2017). Homotopy analysis solution to thermal radiation effects on MHD boundary layer flow and heat transfer towards an inclined plate with convective boundary conditions. *International Journal of Applied and Computational Mathematics*, *3*, 2533-2552.

Shoaib, M., Raja, M. A. Z., Sabir, M. T., Islam, S., Shah, Z., Kumam, P., & Alrabaiah, H. (2020). Numerical investigation for rotating flow of MHD hybrid nanofluid with thermal radiation over a stretching sheet. *Scientific Reports*, *10*(1), 18533.

Soomro, F. A., Usman, M., El-Sapa, S., Hamid, M., & Haq, R. U. (2022). Numerical study of heat transfer performance of MHD Al2O3-Cu/water hybrid nanofluid flow over inclined surface. *Archive of Applied Mechanics*, *92*(9), 2757-2765.

Wahid, N. S., Arifin, N. M., Khashi'ie, N. S., Pop, I., Bachok, N., & Hafidzuddin, M. E. H. (2022). MHD mixed convection flow of a hybrid nanofluid past a permeable vertical flat plate with thermal radiation effect. *Alexandria Engineering Journal*, *61*(4), 3323-3333.

Waini, I., Ishak, A., Groşan, T., & Pop, I. (2020). Mixed convection of a hybrid nanofluid flow along a vertical surface embedded in a porous medium. *International Communications in Heat and Mass Transfer*, *114*, 104565.

Weidman, P. D., Kubitschek, D. G., & Davis, A. M. J. (2006). The effect of transpiration on self-similar boundary layer flow over moving surfaces. *International journal of engineering science*, *44*(11-12), 730-737.

Zaimi, K., & Ishak, A. (2016). Stagnation-point flow towards a stretching vertical sheet with slip effects. *Mathematics*, *4*(2), 27.